ABC Triblock Copolymer Micelle-Like Aggregates in Selective Solvents for A and C

Gabriel Njikang, Dehui Han, Jian Wang, and Guojun Liu*

Department of Chemistry, Queen's University, 90 Bader Lane, Kingston, Ontario, Canada K7L 3N6

Received August 19, 2008; Revised Manuscript Received October 14, 2008

ABSTRACT: Interesting self-assembly behavior of an ABC triblock copolymer in selective solvents for the terminal A and C blocks is reported. The triblock copolymer consists of poly(*tert*-butyl acrylate)-*block*-poly(2-cinnamoyloxyethyl methacrylate)-*block*-poly(glyceryl monomethacrylate) or PtBA-*b*-PCEMA-*b*-PGMA, with 107 tBA units, 193 CEMA units, and 115 GMA units. The solvents used are pyridine/methanol with methanol volume fraction f_{MeOH} between 80 and 100%. While pyridine is a good solvent for all of the three blocks, methanol is selective for PtBA and PGMA. At $f_{MeOH} = 80\%$ and $f_{MeOH} = 90\%$ and at 50 °C, spherical and cylindrical micelles with PtBA and PGMA coronal chains are formed. At $f_{MeOH} = 95\%$, vesicles are formed. Grafted on the outer surface of the vesicles are mostly the PGMA chains and some PtBA chains. The PtBA chains are found by atomic force microscopy and transmission electron microscopy to segregate from the PGMA chains to form circular patches. At $f_{MeOH} = 100\%$, tubular micelle-like aggregates (MAs) coexisted with vesicular MAs. While there have been many reports on morphologies of block copolymer MAs, reports on MAs of ABC triblock copolymers in selective solvents for A and C are rare. Also, there have been very few reports on tubular MAs and MAs with segregated surface chains. These combinations make results of this study unique.

I. Introduction

The association of block copolymers in block-selective solvents yields micelle-like aggregates (MAs) with shapes ranging from spheres[1,2] to cylinders,[3−8] donuts,[9−11] vesicles,[4,9,12,13] and tubes.[14,15] The shape diversity of such aggregates facilitates their applications in nanofabrication,[16−18] lithography,[19−21] cell culturing,[22,23] and drug delivery.[24−26] Most of past morphological studies of MAs were performed using diblock copolymers. When linear ABC triblock copolymers were studied,[27,28] solvents selective for one terminal block (A or C) or two consecutive blocks (A and B or B and C) were typically used.[29−34] With rare exceptions for linear ABC triblock copolymers[35−37] and with exceptions for mikto-arm ABC triblock copolymers,[38,39] the use of such solvents led to the formation core−shell−corona spheres[29,40] or cylinders.[18,41] Our group has been interested in particles with segregated surface chains. Aside from developing methods to bring different diblock copolymers together to form particles with segregated surface chains,[42−44] a direct method for such particles has been to prepare MAs from ABC triblock copolymers in block-selective solvents for the terminal A and C blocks.[45] The A and C blocks used before were not highly incompatible, and their surface chain segregation was absent or not obvious.[45−47] We report in this paper the preparation of MAs from an ABC triblock copolymer with highly incompatible A and C blocks in binary mixtures consisting of a solvent and a block-selective solvent. We discuss its rich morphologies and the interesting segregation patterns of the A and C chains on the surfaces of the vesicles and nanotubes.

Specifically, the triblock copolymer used was poly(*tert*-butyl acrylate)-*block*-poly(2-cinnamoyloxyethyl methacrylate)-*block*-poly(glyceryl monomethacrylate) or PtBA-*b*-PCEMA-*b*-PGMA. With PGMA being hydrophilic and PtBA being hydrophobic, the two terminal blocks should be highly incompatible. The MAs were prepared in pyridine/methanol (Py/MeOH) with different MeOH volume fraction f_{MeOH}. Here Py was a mutual solvent for all of the three blocks of the copolymer and MeOH was selective toward PtBA and PGMA. As f_{MeOH} increased from 80 to 100%, the morphology of the MAs changed from spheres to cylinders, vesicles, and tubes.

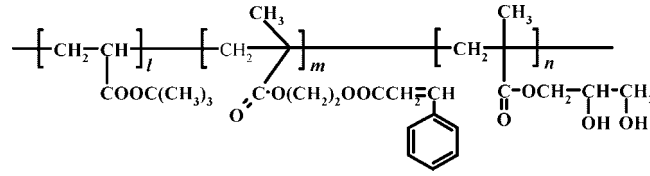

While there have been many reports on morphologies of block copolymer MAs, reports on self-assembled tubular MAs[14,15,48−51] are rare despite reports on their preparation from the chemical processing, involving the cross-linking and sculpting of selective domains, of ABC triblock copolymers cylindrical MAs.[41,52,53] Also, reports on MAs of ABC triblock copolymers in selective solvents for A and C and on MAs with segregated surface chains are rare. These combinations make results of this study unique.

II. Experimental Section

Materials. Anhydrous diethyl ether, methanol, and methylene chloride were of reagent grade from Fisher Scientific and were used without further purification. Pyridine (99.9%) from Fisher Scientific was dried by filtration through alumina columns of an Innovative Technology system. 3-Aminopropyltrimethoxysilane (97%, APT-MS), succinic anhydride (99+%), trifluoroacetic acid (99%), cinnamoyl chloride (98% and dominantly *trans*), and triethylsilane (99%) were purchased from Aldrich and used as received. Spectra/Por dialysis tubes used had a molecular weight cutoff of 12000−14000.

PtBA-*b*-PCEMA-*b*-PGMA. The triblock copolymer was derived from a precursor prepared by anionic polymerization. Since the syntheses and characterization of the same family of triblock copolymers with different compositions have been described before,[18,54] they are thus not repeated here.

MA Preparation. MAs were prepared by dispersing at 50 °C the triblock copolymer at 1.0 mg/mL in pyridine/methanol at a given f_{MeOH}. The samples were stirred for 2 d before any analysis.

Triblock Thermal Stability. The stability of the PCEMA block of the PtBA-*b*-PCEMA-*b*-PGMA copolymer against thermal cross-linking during the 2 d of heating at 50 °C to prepare the MAs was

* Corresponding author.

10.1021/ma801882r CCC: $40.75
Published on Web 11/18/2008

established by comparing the size-exclusion chromatograms of the copolymers that were subjected and not subjected to the thermal treatment. The two samples used for this test was each at 3.0 mL and 1.0 mg/mL. The f_{MeOH} used were 95 and 100%, respectively. After the samples were heated for 2 d, the solvents were removed by rota-evaporation. The samples were further dried for 30 min in a vacuum oven before they were dissolved in 0.5 mL of DMF containing 0.25% of tetrabutylammonium bromide and injected for size-exclusion chromatography (SEC) analysis.

The SEC analysis was performed on a Waters 515 system equipped with three columns (styragel HR 5E and 4E columns and an μStyragel 500 Å column) and a differential refractometer (Water 2410). The system was calibrated by monodisperse polystyrene standards. The eluant used was DMF containing 0.25% tetrabutylammonium bromide at a flow rate of 0.4 mL/min.

PCEMA Cross-Linking and PtBA Hydrolysis. The PCEMA domains of MAs in pyridine/MeOH were cross-linked at 50 °C by a focus beam that had passed a 270 nm cutoff filter from a 500 W mercury lamp powered by an Oriel 6128 power supply. To hydrolyze the tBA units 21 mg of a cross-linked spherical MA sample prepared at $f_{MeOH} = 80\%$ was first dialyzed against MeOH for solvent switching. The MA solution in methanol was concentrated to 2 mL by rota-evaporation before addition into 20 mL of diethyl ether to precipitate the cross-linked MAs. After centrifuging and decanting, the precipitate was rinsed with 5 mL of diethyl ether thrice and then dispersed in 2 mL of methylene chloride. To the dispersion was then added 10 μL of triethylsilane and 0.67 mL of trifluoroacetic acid. The mixture was stirred overnight before excess diethyl ether was added to precipitate the MAs. The precipitate was washed thrice with ether before it was redispersed in 10 mL of water.

Reacting the Vesicles with Succinic Anhydride. Succination of hydroxyl groups has been reported by our group on multiple occasions.[44,55] To succinate the vesicles, 10 mg of cross-linked vesicles freshly precipitated from diethyl ether was dissolved in 2 mL of pyridine in a 50 mL round-bottom flask. To the vesicle solution containing 0.030 mmol of PGMA hydroxyl groups was added 44 mg or 0.44 mmol of succinic anhydride dissolved in 1 mL of pyridine. The mixture was stirred magnetically overnight before it was dialyzed against water to remove small-molecule reagents and side products.

DLS Measurements. Dynamic light scattering (DLS) measurements were carried out at room temperature on a Brookhaven BI-200 SM instrument equipped with a BI-9000AT digital correlator and a He−Ne laser (632.8 nm). Measurements were done at 90°. Samples were clarified by filtration through 0.2 and 1.5 μm Titan2 regenerated cellulose filters for the spherical and vesicular MAs, respectively. The data were treated by the Cumulant method[56] to yield particle hydrodynamic diameter d_h and polydispersity K_2^2/K_4. The refractive index n_r of a Py/MeOH mixture was estimated from[57]

$$n_r = n_{r1} f_{MeOH} + n_{r2}(1 - f_{MeOH}) \quad (1)$$

where n_{r1} and n_{r2} are the refractive indices of MeOH and pyridine, respectively. The viscosity η of a solvent mixture was calculated using[58]

$$\ln \eta = \phi_1 \ln \eta_1 + \phi_2 \ln \eta_2 \quad (2)$$

with η_1 and η_2 being the viscosity of solvents 1 and 2, respectively, and ϕ_1 and ϕ_2 being the molar fractions for solvents 1 and 2.

TEM Measurements. Transmission electron microscopy (TEM) measurements were carried out on a Hitachi H-7000 instrument operated at 75 kV. The specimens for TEM were prepared by aspirating the sample solutions on carbon- or nitrocellulose-coated copper grids. To stain the PCEMA domains, the specimens were stained by either OsO_4 or RuO_4 vapor from 30 min to 2 h.

Two methods were used to stain the carboxyl groups. Method one involved aspirating first a sample on a 1 × 1 cm^2 carbon film supported on mica. The specimen was then stained with 3 drops of uranyl acetate or $UO_2(Ac)_2$ solution in methanol at 50 mg/mL for 30 min. Filter paper was used afterward to remove the excess staining solution. Further removal of the excess staining agent was achieved by rinsing each specimen 10 times using a total of 2.0 mL of MeOH/H_2O at v/v = 8/2. The carbon film was finally floated on water surface and transferred onto a TEM grid. In method two, 3 volumes of the sample solution were directly mixed with 2 volumes of uranyl acetate solution in methanol. The mixture was stirred for 2 h before it was dialyzed against water for 48 h with water changed 8 times to remove excess uranyl acetate. The solution was then aspirated onto a TEM grid.

Table 1. Molecular Properties of PtBA-*b*-PCEMA-*b*-PSMA

SEC M_w/M_n	dn_r/dc (mL/g)	LS $10^{-4}\times$ M_w(g/mol)	NMR *l/m/n*	l_w	m_w	n_w
1.06	0.181	8.7	0.93/1.7/1.0	107	193	115

Surface Modification of Silicon Wafers. Silicon wafers were cleaned by sonicating them for 30 min, in a 1% MICRO-90 detergent cleaning solution, obtained from International Products Corporation. The cleaned wafers were rinsed first with excess distilled water and later with acetone before they were dried in a stream of nitrogen. The cleaned wafers were then treated with piranha solution (70% by volume of sulfuric acid and 30% by volume of hydrogen peroxide) at 80 °C for 3 h to introduce hydroxyl groups. After rinsing with distilled water and acetone, the silicon wafers were dried in a stream of nitrogen. Surface amino groups were introduced by treating silicon wafers using aminopropyltriethylsilane, as described previously.[59]

AFM Measurements. Tapping mode atomic force microscopy (AFM) studies were performed on a Veeco Multimode Microscope equipped with a Nanoscope IIIa Controller. For ambient AFM measurements, silicon tips with force constant and oscillating frequency at about 40 N/m and about 300 kHz were used. Specimens for ambient AFM measurements were prepared by aspirating sample solutions on to either freshly cleaved mica or cleaned silicon wafer.

Solution AFM was performed using DNP-S-NP Series Veeco Probes with force constant and oscillating frequency at about 0.58 N/m and about 57 kHz, respectively. An aqueous solution of the succinated MAs with pH adjusted to 7.4 was dropped on the surface-modified silicon wafer and equilibratred for 1 h to allow for the anchoring of the succinated MAs before an AFM measurement.

III. Results and Discussion

Triblock Copolymer Characterization. The PtBA-*b*-PCEMA-*b*-PGMA sample was characterized in the PtBA-*b*-PCEMA-*b*-PSMA form for the similar solubility between PtBA, PCEMA, and PSMA, where PSMA denotes poly(solketal methacrylate).[52] The repeat unit number ratios *l/m/n* were determined from comparing the ^{1}H NMR peaks of the three blocks of the copolymer. The specific refractive index increment dn_r/dc and the light scattering (LS) molecular weight M_w of the copolymer were determined in butanone. The polydispersity index M_w/M_n of the sample was measured by SEC in THF based on polystyrene standards. By combining the NMR *l/m/n* and LS M_w values, the weight-average repeat unit numbers l_w, m_w, and n_w for the PtBA, PCEMA, and PSMA blocks were calculated to be 107, 193, and 115, respectively (Table 1).

MAs at Different f_{MeOH}. MAs were prepared by stirring the triblock copolymer at 50 °C for at least 2 d in Py/MeOH of a given f_{MeOH}. This temperature was chosen because the triblock dispersed very slowly at room temperature in Py/MeOH at $f_{MeOH} = 95$ and 100%. Then, the MAs prepared at these two f_{MeOH}'s at room temperature were not well defined and contained large aggregates.

The heating protocol was acceptable because the PCEMA block of the copolymer was shown by SEC analysis not to undergo any noticeable thermal cross-linking. For the original

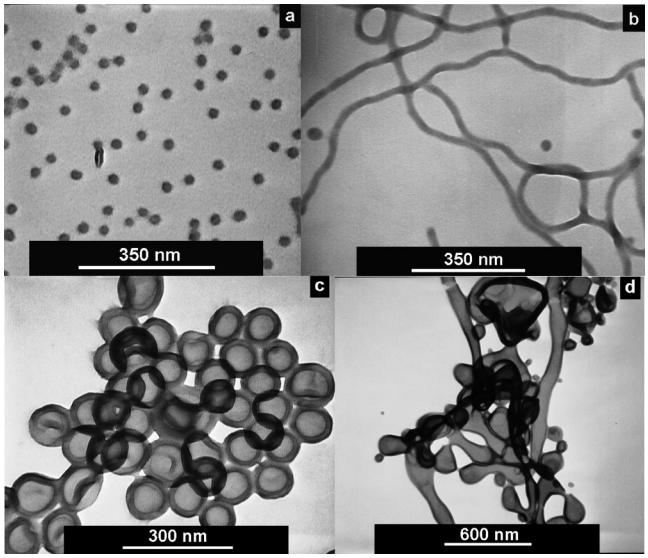

Figure 1. TEM images of MAs aspirated from pyridine/methanol at methanol volume fractions of 80 (a), 90 (b), 95 (c), and 100% (d). The spherical MA sample was stained by RuO_4 vapor, and the other samples were stained by OsO_4 vapor.

or unheated sample, the PS-equivalent SEC M_w and M_w/M_n values measured using DMF as the eluant were $(1.62 \pm 0.01) \times 10^5$ g/mol and 1.31 ± 0.01, respectively, based on the results of two injections. The corresponding values for a sample heated in Py/MeOH at $f_{MeOH} = 95\%$ were $(1.62 \pm 0.01) \times 10^5$ g/mol and 1.29 ± 0.01, respectively, and those for a sample heated at $f_{MeOH} = 100\%$ were $(1.60 \pm 0.01) \times 10^5$ g/mol and 1.31 ± 0.01, respectively. The SEC M_w and M_w/M_n values did not change within experimental error with sample heating. The M_w/M_n values here appeared artificially high because this set of columns for SEC analysis using DMF as the eluant was partially damaged.

Figure 1 shows TEM images of MAs aspirated from Py/MeOH with f_{MeOH} at 80, 90, 95, and 100% on carbon-coated copper grids and stained by the PCEMA-selective OsO_4 or RuO_4. The MA morphologies obviously changed with f_{MeOH}. Only spherical MAs were seen at $f_{MeOH} = 80\%$. At $f_{MeOH} = 90\%$, mostly cylindrical MAs and a few spherical MAs coexisted. Exclusively, vesicles were found at $f_{MeOH} = 95\%$. In methanol, the MAs consisted of a mixture of vesicles, tubes, and branched tubes.

MA morphological transition from spheres to cylinders and then to vesicles in solvent/selective solvent binary mixtures with increasing selective solvent content has been observed on many occasions for diblock copolymers.[9,60,61] Shen and Eisenberg[62] observed this trend, for example, for PS_{310}-*b*-PAA_{52} consisting of 310 styrene units and 52 acrylic acid units in dioxane/water, when the PAA-selective water weight fraction increased from 5 to 45%. Ding et al.[9] observed spherical micelle formation from PS_{1250}-*b*-$PCEMA_{160}$ in tetrahydrofuran/cyclopentane at a tetrahydrofuran volume fraction of 97%. In cyclopentane, which was selective for PS, cylindrical micelles were formed.

Increases in the interfacial energy G_{in} between the micellar core and the solvent phase with increasing block-selective solvent content have been accepted as the cause for such micellar morphological transitions. To decrease G_{in}, the size of the micelles increases initially with increasing block-selective solvent content as predicted theoretically[63,64] and verified experimentally.[60,65] This size increase is accompanied by increases in the stretching energies G_l and G_r of the coronal chains and core chains. Above a critical micellar size, a system decreases its total G by going through a morphological transition.

Table 2. Characteristics of Different MAs

MA type	d_{TEM}/nm[a]	δ_w/nm	d_{AFM}/nm[a]	h_{AFM}/nm	d_{DLS}/nm[b]	DLS[b] K_2^2/K_4
spherical	24 ± 3		56 ± 5	14 ± 1	57 ± 1	0.11 ± 0.02
cylindrical	26 ± 3		54 ± 7	24 ± 2		
vesicular	116 ± 14	20 ± 2	168 ± 17	90 ± 11	177 ± 2	0.04 ± 0.03
tubular	111 ± 19	20 ± 4	126 ± 20	70 ± 8		

[a] The samples were aspirated from pyridine/methanol at their formation. f_{MeOH}s. [b] DLS was performed at their formation, f_{MeOH}s. The standard deviations here denote data precision and is different from those appearing in other columns.

Interestingly, the PtBA-*b*-PCEMA-*b*-PGMA MAs have a similar morphological variation trend with selective solvent content as diblock copolymer MAs. Even more interesting has been the observation of tubular MAs for the triblock copolymer.[48] Self-assembled nanotubes have been reported so far for very few diblock copolymer systems and for one ABA triblock copolymer system.[14,15,48,49,51] We are not aware of reports on self-assembled nanotubes from ABC triblock copolymers. For coil-coil diblock copolymers, nanotubes are formed at very low soluble block weight fractions, for example, <5%.[14] Here tubular MAs were formed at a PGMA and PtBA total weight fraction of 39%. Such tubular MAs should be much more dispersible in solvents for their potential controlled delivery and release application.

Spherical MAs. Spherical MAs were formed in Py/MeOH at $f_{MeOH} = 80\%$, and a TEM image of such aspirated MAs has been shown in Figure 1a. Since the specimen was stained by the PCEMA-selective RuO_4, the uniformly sized circular objects of Figure 1a must be projections of the spherical PCEMA cores. Averaging over all the particles in Figure 1a, we obtained a TEM core diameter d_{TEM} of 24 ± 3 nm as listed in Table 2.

Figure 2a shows an AFM topography image of the MAs aspirated. The MAs appear hemispherical because the AFM tip could not probe the bottom half of the spheres. The particles have an average diameter d_{AFM} of 56 ± 5 nm and height h_{AFM} of 14 ± 1 nm. We have also determined by DLS an average diameter d_{DLS} of 57 ± 1 nm and a polydispersity index K_2^2/K_4 of 0.11 ± 0.02 for the MAs.

For nondeformable core−shell spheres, the TEM diameter of the whole sphere including the shell should be the same as the AFM height. The fact that the PCEMA core TEM diameter d_{TEM} of 24 ± 3 nm was substantially larger than the h_{AFM} value of 14 ± 1 nm suggests the substantial flattening of the particles on the silicon substrate and TEM grid. Thus, the radius of a nonflattened core should be less than the TEM radius of 12 nm. The particle cores flattened upon contact probably because they were then highly swollen.

At 193 units, the PCEMA block has a fully stretched chain length of 49 nm. Assuming a characteristics ratio C_∞ of 6.0, a typical value for atactic poly(methyl methacrylate),[66] the root-mean-square end-to-end distance of such a chain in the unperturbed state was estimated to be 7.4 nm. The core chains of spherical micelles should normally be more stretched than those in the unperturbed state.[6,67,68] We cannot conclude this with certainty here because we do not know by how much smaller the actual radius of the spherical MAs was than the TEM radius 12 nm. This is different from the diblock copolymer spherical micelle case. At a similar soluble to insoluble block weight ratio and insoluble block length, the core diameter of a diblock spherical micelle sample would have been substantially larger.[6,68] This smaller triblock copolymer micelle size is common and has been seen before by others[27,47] and by us.[45] This reduced MA size and thus aggregation number should have resulted from the stronger repulsion between the dissimilar A and C coronal chains.

The h_{AFM} value is normally less than d_{AFM} because of the tip width effect and also for particle flattening. The d_{DLS} value is

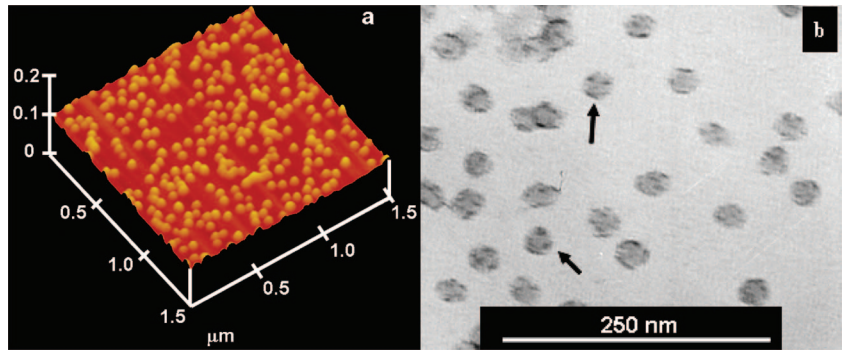

Figure 2. AFM topography (a) and TEM (b) images of spherical MAs aspirated from Py/MeOH at $f_{MeOH} = 80\%$. Before aspiration, the TEM sample was photolyzed to cross-link the PCEMA core and treated by trifluoroacetic acid to hydrolyze PtBA. The resultant PAA chains were stained by $UO_2(Ac)_2$.

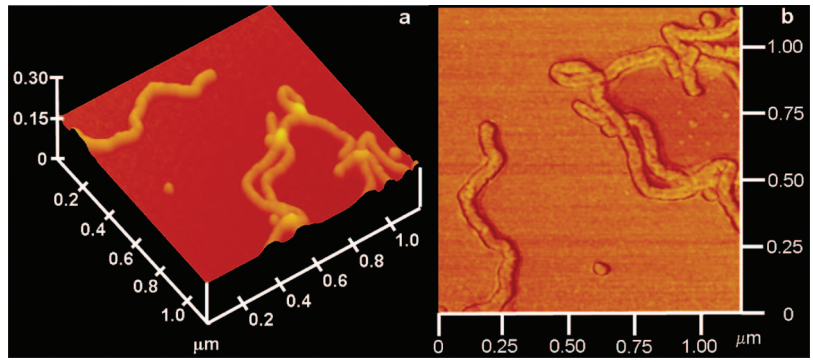

Figure 3. AFM topography (a) and phase (b) images of cylindrical MAs aspirated from Py/MeOH at $f_{MeOH} = 90\%$.

larger than d_{TEM} because DLS measures the size of the whole micelle including the PGMA and PtBA corona. Also, DLS measures the size of the swollen particles and TEM measures that of the dry particles.

To probe the distribution of the corona A and C chains, we irradiated the spherical MAs in pyridine/MeOH to cross-link the PCEMA core. We then hydrolyzed the coronal PtBA chains to PAA chains. The resultant PAA chains were stained by $UO_2(Ac)_2$ for enhancement of contrast between PAA and PGMA. Figure 2b shows a TEM image of the PCEMA-cross-linked and PtBA-hydrolyzed spheres aspirated from water.

Distinctively dark dots corresponding to stained PAA domains are seen on some particles (two marked by arrows) in Figure 2b. This suggests the segregation of the PAA and PGMA chains. This should, however, be treated with skepticism because the size of the PAA domains was comparable to the radius of gyration of a PAA chain. Such small domains could have formed due to the collapsing of a single PAA chain or from the clustering of several PAA chains during TEM specimen preparation or solvent evaporation. These several chains did not have to be immediate neighbors in their solvated state.

Cylindrical MAs. Mostly cylindrical MAs plus occasional spherical MAs were seen in samples aspirated from Py/MeOH at $f_{MeOH} = 90\%$. Averaging over 93 sections of five cylindrical MAs in Figure 1b, we obtained a TEM PCEMA core diameter d_{TEM} of 26 ± 3 nm (Table 2). Figure 3a shows an AFM topography image of the cylindrical MAs. The average AFM diameter d_{AFM} and height h_{AFM} values were 54 ± 7 and 24 ± 2 nm, respectively.

The comparable d_{TEM} and h_{AFM} values suggests a lower degree of particle flattening than the spherical MAs after their aspiration on solid substrates. This is reasonable as the cores would be less swollen here for the higher f_{MeOH} value.

Figure 3b shows an AFM phase image of the cylindrical MAs. Because the AFM image was obtained at a minimal force required for stable imaging, we doubt that the tip penetrated the coronal layer and probed the PCEMA core. If only the surface chains were probed, the phase contrast in Figure 3b must be due to the different viscoelastic properties of the segregated surface PtBA and PGMA chains. This conclusion should again be treated with skepticism as the segregated domains were too small to be discerned with confidence. We have also cross-linked the PCEMA cores and hydrolyzed the coronal PtBA chains of the cylindrical MAs. The resultant PAA chains were then stained by $UO_2(Ac)_2$. Again, the TEM images did not allow a definitive conclusion about the segregation of the PGMA and PAA chains.

Vesicular MAs. Figure 4a shows a 3D AFM image of a MA sample aspirated from Py/MeOH at $f_{MeOH} = 95\%$. Spherical particles coexisted with "bowl-shaped" particles. We also imaged the particles in water. This required the surface modification of silicon wafers, which were used as the AFM imaging substrate, for amine group introduction. It also required the introduction of carboxyl groups onto the surfaces of the particles. The latter was achieved by cross-linking the PCEMA shell of the particles first and then reacting the hydroxyl groups of the PGMA chains with succinic anhydride. The electrostatic interaction between the amine and carboxyl groups facilitated the pinning down of the particles on to silicon surfaces for imaging. Figure 4b shows a solution AFM image of the MAs obtained under water.

MA clumps were preferentially imaged by solution AFM probably because they were more easily pinned down by the substrate. The MA clump image clearly shows that all discernible particles were spherical. Thus, the MAs at $f_{MeOH} = 95\%$ must be vesicles and the bowl-shaped particles seen by ambient AFM were formed probably due to the partial collapse of the hollow particles after evaporation of solvent from the cores.

The spherical vesicular particles of Figure 4a had an average height h_{AFM} of 90 ± 11 nm and a diameter d_{AFM} of 168 ± 17 nm. These are far larger than those of the spherical particles

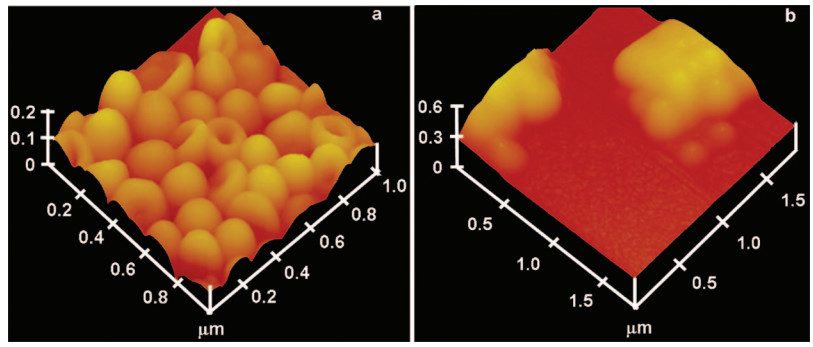

Figure 4. Solid (a) and solution (b) AFM topography images of vesicular MAs formed at $f_{MeOH} = 95\%$. The vesicles in image b were cross-linked and reacted with succinic anhydride before their anchoring on amine-modified silicon wafer surface.

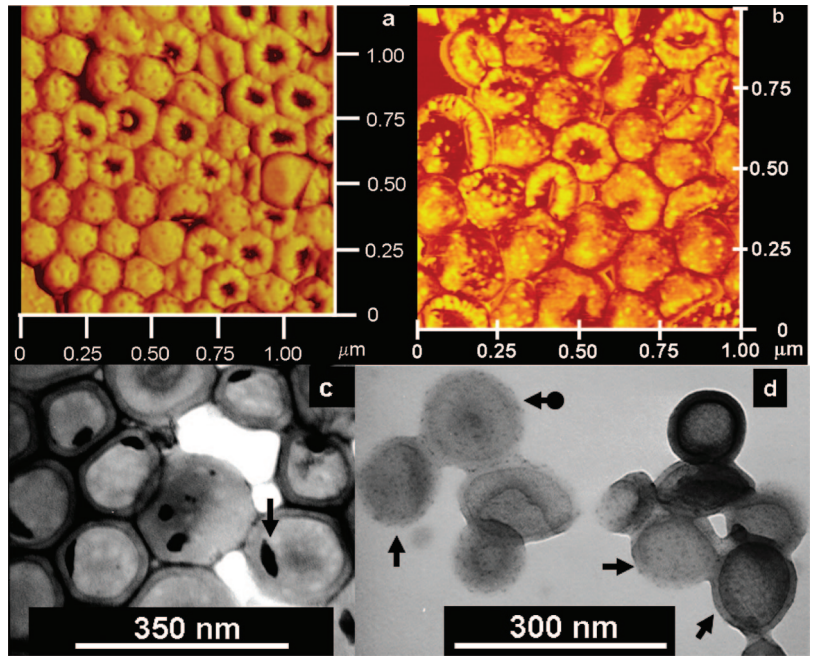

Figure 5. AFM phase (a and b) and TEM (c and d) images of the PtBA-*b*-PCEMA-*b*-PGMA vesicles (a) and their derivatives (b-d). Images b and d are for PCEMA cross-linked and PtBA-hydrolyzed vesicles, and image c is for PtBA-*b*-PCEMA-*b*-PSGMA vesicles. Both of the TEM specimens were stained by $UO_2(Ac)_2$.

prepared at $f_{MeOH} = 80\%$. The vesicle assignment suggests that the dark rim and the gray core of each circular object of Figure 1c were projections of the PCEMA shell and the vesicle cavity, respectively. Based on these, our quantitative analysis of many particles yielded an average TEM diameter d_{TEM} of 116 ± 14 nm for the vesicles including the PCEMA shell (Table 2). The thickness δ_w of the PCEMA shell was 20 ± 2 nm. We have also performed DLS analysis of the vesicles in Py/MeOH at $f_{MeOH} = 95\%$ and yielded a diameter d_{DLS} of 177 ± 2 nm and a polydispersity index of 0.04 ± 0.03 for the vesicles.

That d_{TEM} was larger than h_{AFM} suggests again the flattening of the vesicles after their aspiration from solution. d_{DLS} was larger than d_{TEM} because DLS probed the size of the whole solvated vesicles and TEM yielded the diameter of the flattened dry vesicles. The low DLS polydispersity value was in agreement with the narrow vesicle size distribution that was seen by AFM and TEM. The δ_w value of 20 ± 2 nm suggests some stretching of the PCEMA chains, a phenomenon typical for block copolymer vesicles.[69]

The distribution of coronal chains on the two surfaces of a vesicle was very intriguing. Eisenberg and co-workers[70−72] and Stoenescu and Meier[73] showed by fluorescence quenching experiments that the larger coronal block of A and C of ABC copolymers segregated preferentially on the outer surface. Based on the repeat unit numbers of 107 and 115 for the PtBA and PGMA blocks and the larger size of each GMA unit, our suspicion was that PGMA would preferentially segregate on the outer surfaces.

The occurrence of PGMA chains on the outer surface was supported by the following observations: First, the vesicles after PCEMA cross-linking and dialysis against water remained dispersible in water, which was selective for PGMA. Second, the PCEMA-cross-linked vesicles could be imaged on the amine-modified silicon wafers after treatment with succinic anhydride, which reacted with PGMA to generate carboxyl groups.

Figures 5a shows an AFM phase image of PtBA-*b*-PCEMA-*b*-PGMA vesicles aspirated on silicon from Py/MeOH at $f_{MeOH} = 95\%$. This vesicle sample was also photolyzed to cross-link PCEMA and treated by trifluoroacetic acid to hydrolyze PtBA. Figures 5b shows an AFM phase image of the resultant sample, and its TEM image after staining by $UO_2(Ac)_2$ is shown in Figure 5d. The PCEMA-cross-linked PtBA-*b*-PCEMA-*b*-PGMA vesicles were reacted also with succinic anhydride to produce PtBA-*b*-PCEMA-*b*-PSGMA vesicles with PSGMA denoting poly(succinated glyceryl monomethacrylate). Figure 5c shows a TEM image of the PtBA-*b*-PCEMA-*b*-PSGMA vesicles stained by $UO_2(Ac)_2$.

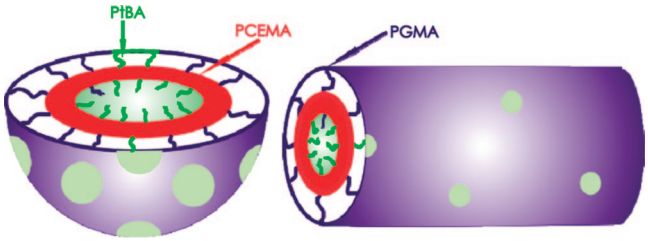

Figure 6. Cross-sectional schematics of structures of vesicular (left) and tubular (right) MAs.

Because the interpretation of phase contrast on rugged surfaces is tricky,[74] we concentrate our discussion on these spherical rather than bowl-shaped particles in Figure 5a and b. On these particles dark dots of an average diameter of 18 ± 5 nm are seen in Figure 5a, and bright dots of an average diameter of 19 ± 4 nm are seen in Figure 5b. Because no holes are seen on the walls of the vesicles from Figures 1c and 4, the phase contrast must be due to the different viscoelastic properties of two polymers on the vesicle surfaces. The inversion of the phase contrast[74,75] under essentially identical imaging conditions from Figure 5a to b must be due to a modulus change from PtBA to PAA. As expected, the PtBA to PAA conversion did not change the domain size.

Light circular spots with a diameter 16 ± 3 nm are seen in Figure 5c for the PtBA-*b*-PCEMA-*b*-PSGMA vesicles. Since PSGMA was stained by $UO_2(Ac)_2$, these white spots must correspond to the unstained PtBA domains. The TEM spot sizes are smaller than those from AFM most likely for the tip size effect in AFM. The density of light spots is higher in Figure 5c than those of the circular domains in Figures 5a and 5b probably because the circular PtBA domains on the surface of both the top and bottom hemispheres of a vesicle were imaged by TEM. On the other hand, AFM probed the surface of only the top hemisphere of a vesicle.

The segregation of PtBA chains mostly on the inner surface can be appreciated from the following observations. First, dark $UO_2(Ac)_2$ agglomerates (one marked by arrow) were seen in the core of the PtBA-*b*-PCEMA-*b*-PSGMA vesicles of Figure 5c but not in the cores of PAA-*b*-PCEMA-*b*-PGMA vesicles of Figure 5d. Second, the core of the PAA-*b*-PCEMA-*b*-PGMA vesicles was more heavily stained by $UO_2(Ac)_2$ than the corona in Figure 5d. Agglomerates of $UO_2(Ac)_2$ were seen in the cores of the PtBA-*b*-PCEMA-*b*-PSGMA vesicles because $UO_2(Ac)_2$ did not bind with PtBA and crystallized out during solvent evaporation. UO_2^{2+} spread more uniformly in the cores of PAA-*b*-PCEMA-*b*-PGMA vesicles because it complexed with the AA groups. The more heavy staining of the PAA core by $UO_2(Ac)_2$ is evident for the three vesicles marked by regular arrows in Figure 5d.

Dark dots associated with the concentration of UO_2^{2+} are seen on the PAA-*b*-PCEMA-*b*-PGMA vesicles of Figure 5d. That at least some of dots occurred on the outer surface of the vesicles is best seen in the particle marked by an arrow with a round end. The dark dots occurred on the outer surface because of the presence of PAA domains as seen in Figures 5b–5c. The dots here are, however, much smaller than those there. Our suspicion is that not each AA unit was bound to UO_2^{2+} and UO_2^{2+} was not uniformly distributed inside the PAA domains. After all, these stained samples were rinsed extensively with water to remove physically trapped UO_2^{2+} and some UO_2^{2+} sorbed by AA groups might have also been removed during this process.

Figure 6a depicts the vesicle structure of our current understanding. While we are confident about the dominance of the PtBA chains on the core surface, there must be some PGMA chains there as well. This is depicted by drawing a single PGMA chain on the inner surface of the vesicle in Figure 6. Entropy maximization should drive the uniform distribution of PGMA and PtBA on both surfaces. They distributed on the different surfaces to minimize the unfavorable PGMA and PtBA contacts. The packing of the longer chains on the more spacious outer surface also helped reduce the stretching energy of the longer chains. Some PtBA domains occurred on the outer surfaces here probably for the small size difference between the PGMA and PtBA blocks and the difficulty for squeezing all the PtBA chains onto the inner vesicle surface.

The direct visualization of the phase separation between PGMA and PtBA as well as between PGMA and PAA was very interesting. The segregation of PGMA and PtBA into easily detectable domain sizes on the same surface reinforces our prior assertion that these two polymers were highly incompatible.

Tubular MAs. Figure 1d suggests the formation in methanol of tubular MAs together with other types of MAs. Figure 7a shows a close-up view of a tubular MA stained by OsO_4, and Figure 7b shows an AFM topography image of a tubular MA clump obtained under water. For the solution AFM imaging, the MAs were photolyzed to cross-link the PCEMA shell and reacted with succinic anhydride to introduce surface carboxyl groups.

The tubular shape of the MAs is unambiguously seen in Figure 7b. Also clear from the images of Figure 1d and Figure 7 is that some tubes bore undulations. The fact that the undulation was seen even in water suggests that it was inherent to the tubes. Of course, we cannot rule out the possibility that some undulated sections seen by TEM and ambient AFM were formed as a result of tube collapsing during specimen preparation for solvent evaporation.

Undulations have been frequently seen in cylindrical MAs of block copolymers.[67,76] Jain and Bates[76] have attributed undulations in their diblock copolymer cylindrical MAs to a "locally equilibrated structure". Along their line of argument, our triblock copolymer probably had a composition intermediate between those for vesicular and tubular MAs. The rate of chain exchange between different block copolymer MAs was very slow in our system at $f_{MeOH} = 100\%$. Once a tube had been formed, chain exchange between different MAs was essentially impossible. Within the same tube, chains of different compositions (always present due to sample heterogeneity) shuffled their positions to facilitate the formation of tube-like and vesicle-like sections.

The dark rim of the object in Figure 7a must be due to the PCEMA shell. Our quantitative analysis yielded a TEM thickness of 20 ± 4 nm for the shell (Table 2) and a diameter of 111 ± 19 nm for the tubes including the PCEMA shell. Analysis of AFM images obtained of aspirated tubular MAs yielded $h_{AFM} = 70 \pm 8$ nm and $d_{AFM} = 126 \pm 30$ nm. These values are all reasonable when compared with each other as has been discussed for the vesicular and spherical MAs.

Figure 8a shows an AFM phase image of a dried tubular MA sample. The dark dots associated with PtBA domains are still seen on the surfaces of the tubes. Their number per unit surface area has decreased. The fact that PtBA are still mostly located on the inner surface can be appreciated from Figure 8b. Here the sample was cross-linked, the PtBA chains were hydrolyzed, and the resultant PAA chains were stained by $UO_2(Ac)_2$. The stain was mainly concentrated on the inner surface of the marked tube. Thus, the PtBA and PGMA chain distribution in the tubular MAs would be similar to that depicted in the right structure of Figure 6.

The decrease in the density of the PtBA domains on the tubular MA surfaces might be caused by the shrinkage of the PtBA chains with f_{MeOH} increase from 95% to 100%. The

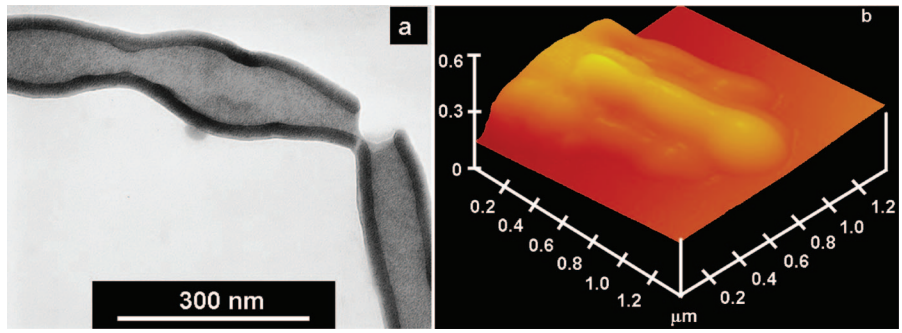

Figure 7. TEM (a) image of a tubular MA aspirated from methanol and solution AFM topography image (b) of tubular MAs in water. The TEM specimen was stained by OsO_4.

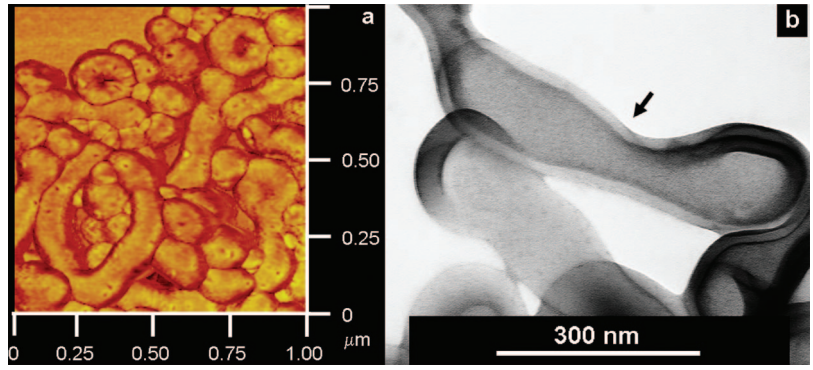

Figure 8. AFM phase (a) and TEM (b) images of nanotubes. To obtain the TEM image, the sample was cross-linked, the PtBA chains were hydrolyzed,and the resultant PAA chains were stained by $UO_2(Ac)_2$.

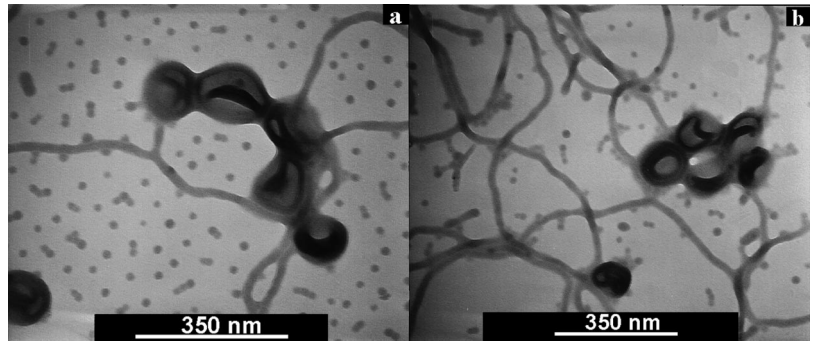

Figure 9. TEM images of transient species aspirated from pyrine/methanol at $f_{MeOH} = 90\%$ 15 (a) and 30 (b) min after pyridine addition to decrease f_{MeOH} from 95 to 90%.

literature solubility parameters δ for Py and MeOH are 21.9 and 29.7 $MPa^{1/2}$, respectively.[66] Our calculations based on group contributions[76,77] yielded δ values of 18.6 and 28.7 $MPa^{1/2}$ for PtBA and PGMA. These parameters indicate that PtBA should assume a less expanded conformation in MeOH than in Py/MeOH and PGMA conformation should be more expanded in MeOH than in Py. This increased PGMA/PtBA size asymmetry should help squeeze more PtBA chains onto the inner surface than at $f_{MeOH} = 95\%$.

Micelles versus MAs. Micelles are self-assembled structures with the lowest Gibbs free energy under a given set of conditions and are thermodynamically favored products. The limited mobility of polymer chains in aggregates may prevent the attainment of the micellar structures. Under such circumstances, the aggregates formed may correspond to kinetically frozen structures. If the stabilization mechanism, kinetic vs thermodynamic stabilization, of an aggregate is unknown, it is normally referred to as a MA.

We suspect that the spherical MAs seen at $f_{MeOH} = 80\%$ were micelles because the PCEMA core chains should be highly mobile at such a high Py content. To know if the cylindrical, vesicular, and tubular MAs were also micelles, we attempted their preparation using methods different from dispersing the copolymer directly at their required f_{MeOH}'s. If the MAs at a given f_{MeOH} were indeed micelles, they should form regardless of how the f_{MeOH} was achieved.

We tried to prepare the cylindrical MAs by preparing vesicular MAs at $f_{MeOH} = 95\%$ first and then adding Py to decrease f_{MeOH} suddenly to 90%. Figure 9 shows two TEM images of the transient species formed after the f_{MeOH} decrease from 95 to 90%.

Before pyridine addition, exclusively vesicles were found in the system as shown in Figure 1c. Only 15 min after Py addition at 50 °C, spherical and cylindrical MAs coexisted with the vesicular MAs (Figure 9a). At 30 min, the population of the spherical and vesicular MAs decreased and that of the cylindrical MAs increased (Figure 9b). At 2 d, essentialy pure cylindrical MAs with occasional spherical and vesicular MAs were obtained. We did not attempt cylindrical MA preparation by starting from spherical micelles because the PCEMA chain

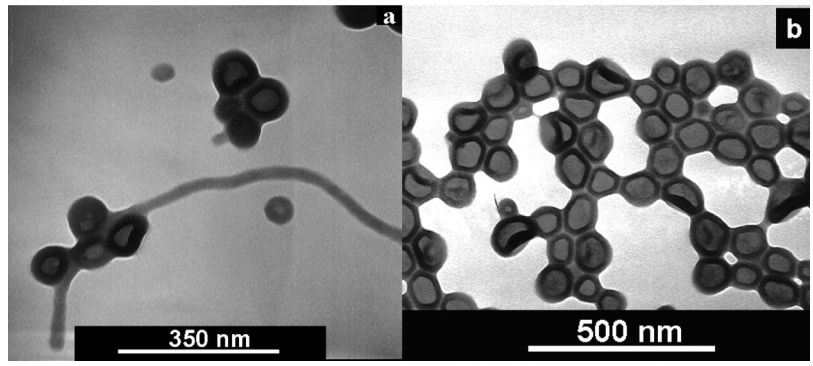

Figure 10. TEM images of samples aspirated from pyrine/methanol 15 min (a) and 4 d (b) after methanol addition to increase f_{MeOH} from 90 to 95%.

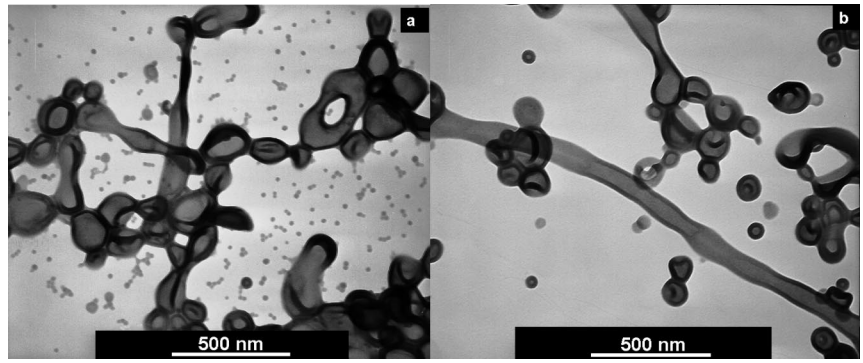

Figure 11. TEM images of samples aspirated from pyrine/methanol 30 min (a) and 5 d (b) after pyridine addition to decrease f_{MeOH} from 100 to 95%.

mobility should be higher between $f_{MeOH} = 80$ and 90% than between $f_{MeOH} = 90$ and 95%, and spherical to cylindrical micelle conversion should be easier than the vesicular to cylindrical MA conversion. Furthermore, the spherical MAs were already produced as seen in Figure 9a from the sudden addition of Py into the vesicular MA solution initially at $f_{MeOH} = 95\%$. Their disappearace and the appearance of the cylindrical MAs suggests their conversion into cylindrical MAs. The fact that the cylindrical MAs were obtained regardless how the final f_{MeOH} of 90% was achieved suggests that the cylindrical MAs were micelles.

Aside from dispersing the triblock copolymer directly in Py/MeOH at $f_{MeOH} = 95\%$, two more approaches were attempted to prepare the vesicular MAs. In one approach, cylindrical MAs were first prepared at $f_{MeOH} = 90\%$ and more MeOH was added to increase suddenly f_{MeOH} to 95%. In the other approach, the copolymer was dispersed in MeOH to yield tubular and other MAs. Pyridine was then added in one aliquot to decrease f_{MeOH} to 95%.

Figure 10 shows TEM images of samples taken 15 min and 4 d after MeOH addition to increase f_{MeOH} from 90 to 95%. At 15 min, cylindrical and vesicular MAs coexisted (Figure 10a). At 30 min, only vesicular MAs were observed and a complete cylinder to vesicule transition was accomplished. At 4 d, the vesicular MAs in Figure 10b reached an average size of 105 ± 17 nm, which is the same within experimental error as that for the visicles shown in Figure 1c.

Figure 11 shows TEM images of samples aspirated from pyrine/methanol 30 min (a) and 5 d (b) after pyridine addition to decrease f_{MeOH} from 100 to 95%. The spherical MAs in the background of Figure 11a had obviously disintegrated and got incorporated or converted into other types of MAs during this time interval. These suggest chain mobility at $f_{MeOH} = 95\%$. The chain mobility is supported also by an increase in the vesicular population in Figure 11b than in Figure 11a. Surprisingly, tubular MAs were still seen in Figure 11b or in samples that were annealed for 20 d after the decrease of f_{MeOH} from 100 to 95%.

We do not have a definitive answer as to why only vesicles were prepared when the copolymer was dispersed directly at $f_{MeOH} = 95\%$ or when $f_{MeOH} = 95\%$ was reached from the lower f_{MeOH} side but a mixture of vesicles and other structures were obtained when $f_{MeOH} = 95\%$ was reached from the higher f_{MeOH} side. Our suspicion is that the tubular MAs were slow to disintegrate for their large size. Once they failed to disintegrate within a given time frame, for example, <10 d, the thermal cross-linking of the PCEMA block, although very slow as has been demonstrated but should occur gradually, would further slow down their disintegration. We thus believe that the vesicular MAs were also micelles. This conclusion was supported by the observation that the vesicle population increased with sample annealing after f_{MeOH} decrease from 100 to 95%. It was supported also by the observation that vesicles were the only morphology from the other two approaches. Furthermore, the final size of the vesicles from the other two approaches was essentially the same.

We also attempted tubular MA mixture preparation starting from vesicular MAs at $f_{MeOH} = 95\%$. Such a solution was then dialyzed against MeOH to remove Py. The resultant vesicular MA sample in MeOH was heated at 50 °C for 15 d. We failed to see any tubular MAs in the resultant sample. Our failure to produce tubular MAs from the second approach, the observation of a multitude of morphologies, and the tube backbone undulation suggest the play of kinetic factors in inducing the formation of these structures in MeOH.

IV. Conclusions

A PtBA-*b*-PCEMA-*b*-PGMA sample was synthesized and characterized. In Py/MeOH at 50 °C and at $f_{MeOH} = 80\%$ and $f_{MeOH} = 90\%$, spherical and cylindrical micelles with PtBA and PGMA

coronal chains were formed. At $f_{MeOH} = 95\%$, vesicles were formed. Grafted on the outer surface of the vesicles were mostly the PGMA chains and some PtBA chains. The PtBA chains were found by atomic force microscopy and transmission electron microscopy to segregate from the PGMA chains to form circular patches. At $f_{MeOH} = 100\%$, tubular MAs were formed together with vesicular MAs. Again, the PGMA chains were found to segregate mostly on the outer surfaces and the PtBA chains mostly on the inner surfaces of the vesicles. Our preparation of a particular type of MAs from different paths at a given f_{MeOH} suggests that the spherical, cylindrical, and vesicular MAs were micelles. We suspect that the tubular MAs were formed for kinetic reasons. While there have been many reports on morphologies of block copolymer MAs, reports on self-assembled tubular MAs and MAs of ABC triblock copolymers in selective solvents for A and C are rare. Also, MAs with segregated surface chains have been rarely reported. These combinations make results of this study unique and interesting.

Acknowledgment. NSERC of Canada is thanked for sponsoring this research. G.L. thanks the Canada Research Chairs program for a research chair position in Materials Science.

References and Notes

(1) Lazzari, M.; Liu, G. J.; Lecommandoux, S. *Block Copolymers in Nanoscience*; Wiley-VCH: Weinheim, Germany, 2006.
(2) Tugar, Z.; Kratochvil, P. *Surf. Colloid Sci.* **1993**, *15*, 1–83.
(3) Price, C. *Pure Appl. Chem.* **1983**, *55*, 1563–1572.
(4) Zhang, L. F.; Eisenberg, A. *Science* **1995**, *268*, 1728–1731.
(5) Cui, H. G.; Chen, Z. Y.; Zhong, S.; Wooley, K. L.; Pochan, D. J. *Science* **2007**, *317*, 647–650.
(6) Tao, J.; Stewart, S.; Liu, G. J.; Yang, M. L. *Macromolecules* **1997**, *30*, 2738–2745.
(7) Jain, S.; Bates, F. S. *Science* **2003**, *300*, 460–464.
(8) Li, Z. B.; Kesselman, E.; Talmon, Y.; Hillmyer, M. A.; Lodge, T. P. *Science* **2004**, *306*, 98–101.
(9) Ding, J. F.; Liu, G. J.; Yang, M. L. *Polymer* **1997**, *38*, 5497–5501.
(10) Zhu, J. T.; Liao, Y. G.; Jiang, W. *Langmuir* **2004**, *20*, 3809–3812.
(11) Chen, Z. Y.; Cui, H. G.; Hales, K.; Li, Z. B.; Qi, K.; Pochan, D. J.; Wooley, K. L. *J. Am. Chem. Soc.* **2005**, *127*, 8592–8593.
(12) Ding, J. F.; Liu, G. J. *Macromolecules* **1997**, *30*, 655–657.
(13) Discher, D. E.; Eisenberg, A. *Science* **2002**, *297*, 967–973.
(14) Yu, K.; Eisenberg, A. *Macromolecules* **1998**, *31*, 3509–3518.
(15) Raez, J.; Manners, I.; Winnik, M. A. *J. Am. Chem. Soc.* **2002**, *124*, 10381–10395.
(16) Massey, J. A.; Winnik, M. A.; Manners, I.; Chan, V. Z. H.; Ostermann, J. M.; Enchelmaier, R.; Spatz, J. P.; Moller, M. *J. Am. Chem. Soc.* **2001**, *123*, 3147–3148.
(17) Liu, G.; Yan, X.; Li, Z.; Zhou, J.; Duncan, S. *J. Am. Chem. Soc.* **2003**, *125*, 14039–45.
(18) Yan, X.; Liu, G.; Li, Z. *J. Am. Chem. Soc.* **2004**, *126*, 10059–66.
(19) Park, M.; Harrison, C.; Chaikin, P. M.; Register, R. A.; Adamson, D. H. *Science* **1997**, *276*, 1401–1404.
(20) Thurn-Albrecht, T.; Schotter, J.; Kastle, C. A.; Emley, N.; Shibauchi, T.; Krusin-Elbaum, L.; Guarini, K.; Black, C. T.; Tuominen, M. T.; Russell, T. P. *Science* **2000**, *290*, 2126–2129.
(21) Li, Z.; Zhao, W.; Liu, Y.; Rafailovich, M. H.; Sokolov, J.; Khougaz, K.; Eisenberg, A.; Lennox, R. B.; Krausch, G. *J. Am. Chem. Soc.* **1996**, *118*, 10892–10893.
(22) Silva, G. A.; Czeisler, C.; Niece, K. L.; Beniash, E.; Harrington, D. A.; Kessler, J. A.; Stupp, S. I. *Science* **2004**, *303*, 1352–1355.
(23) Stupp, S. I. *MRS Bull.* **2005**, *30*, 546–553.
(24) Vriezema, D. M.; Aragones, M. C.; Elemans, J.; Cornelissen, J.; Rowan, A. E.; Nolte, R. J. M. *Chem. Rev.* **2005**, *105*, 1445–1489.
(25) Kataoka, K.; Harada, A.; Nagasaki, Y. *Adv. Drug Delivery Rev.* **2001**, *47*, 113–131.
(26) Savic, R.; Luo, L. B.; Eisenberg, A.; Maysinger, D. *Science* **2003**, *300*, 615–618.
(27) Hadjichristidis, N.; Iatrou, H.; Pitsikalis, M.; Pispas, S.; Avgeropoulos, A. *Prog. Polym. Sci.* **2005**, *30*, 725–782.
(28) Fustin, C. A.; Abetz, V.; Gohy, J. F. *Eur. Phys. J. E* **2005**, *16*, 291–302.
(29) Stewart, S.; Liu, G. J. *Chem. Mater.* **1999**, *11*, 1048–1054.
(30) Kriz, J.; Masar, B.; Plestil, J.; Tuzar, Z.; Pospisil, H.; Doskocilova, D. *Macromolecules* **1998**, *31*, 41–51.
(31) Yu, G. E.; Eisenberg, A. *Macromolecules* **1998**, *31*, 5546–5549.
(32) Ishizone, T.; Sugiyama, K.; Sakano, Y.; Mori, H.; Hirao, A.; Nakahama, S. *Polym. J.* **1999**, *31*, 983–988.
(33) Talingting, M. R.; Munk, P.; Webber, S. E.; Tuzar, Z. *Macromolecules* **1999**, *32*, 1593–1601.
(34) Lei, L. C.; Gohy, J. F.; Willet, N.; Zhang, J. X.; Varshney, S.; Jerome, R. *Macromolecules* **2004**, *37*, 1089–1094.
(35) Zhu, J. T.; Jiang, W. *Macromolecules* **2005**, *38*, 9315–9323.
(36) Zhong, S.; Cui, H. G.; Chen, Z. Y.; Wooley, K. L.; Pochan, D. J. *Soft Matter* **2008**, *4*, 90–93.
(37) Schmalz, M.; Schmelz, J.; Drechsler, M.; Yuan, J.; Walther, A.; Schweimer, K.; Mihut, A. M. *Macrolmolecules* **2008**, *41*, 3235–3242.
(38) Li, Z. B.; Hillmyer, M. A.; Lodge, T. P. *Langmuir* **2006**, *22*, 9409–9417.
(39) Li, Z. B.; Hillmyer, M. A.; Lodge, T. P. *Nano Lett.* **2006**, *6*, 1245–1249.
(40) Njikang, G.; Liu, G.; Gao, J. *Macromolecules* **2007**, *40*, 9174–9180.
(41) Stewart, S.; Liu, G. *Angew. Chem., Int. Ed.* **2000**, *39*, 340–344.
(42) Hu, J. W.; Liu, G. J. *Macromolecules* **2005**, *38*, 8058–8065.
(43) Yan, X. H.; Liu, G. J.; Hu, J. W.; Willson, C. G. *Macromolecules* **2006**, *39*, 1906–1912.
(44) Zheng, R. H.; Liu, G. J.; Yan, X. H. *J. Am. Chem. Soc.* **2005**, *127*, 15358–15359.
(45) Hoppenbrouwers, E.; Li, Z.; Liu, G. J. *Macromolecules* **2003**, *36*, 876–881.
(46) Fernyhough, C. M.; Pantazis, D.; Pispas, S.; Hadjichristidis, N. *Eur. Polym. J.* **2004**, *40*, 237–244.
(47) Tsitsilianis, C.; Sfika, V. *Macromol. Rapid Commun.* **2001**, *22*, 647–651.
(48) Liu, G. J. *Adv. Polym. Sci.* **2008**, *230*, 29–64.
(49) Yu, K.; Zhang, L. F.; Eisenberg, A. *Langmuir* **1996**, *12*, 5980–5984.
(50) Raez, J.; Manners, I.; Winnik, M. A. *Langmuir* **2002**, *18*, 7229–7239.
(51) Grumelard, J.; Taubert, A.; Meier, W. *Chem. Commun.* **2004**, 1462–1463.
(52) Yan, X. H.; Liu, F. T.; Li, Z.; Liu, G. J. *Macromolecules* **2001**, *34*, 9112–9116.
(53) Yan, X. H.; Liu, G. J.; Liu, F. T.; Tang, B. Z.; Peng, H.; Pakhomov, A. B.; Wong, C. Y. *Angew. Chem., Int. Ed.* **2001**, *40*, 3593–3596.
(54) Yan, X. H.; Liu, G. J.; Haeussler, M.; Tang, B. Z. *Chem. Mater.* **2005**, *17*, 6053–6059.
(55) Li, Z.; Liu, G.; Law, S. J.; Sells, T. *Biomacromolecules* **2002**, *3*, 984–90.
(56) Berne, B. J.; Pecora, R. *Dynamic Light Scattering with Applications to Chemistry, Biology, and Physics*; Dover Publications, Inc.: Mineola, NY, 1976.
(57) Huglin, M. B. *Light Scattering from Polymer Solutions*; Academic Press: London, 1972; p 34.
(58) Jouyban, A.; Khoubnasabjafari, M.; Vaez-Gharamaleki, Z.; Fekari, Z.; Acree, W. E. *Chem. Pharm. Bull.* **2005**, *53*, 519–523.
(59) Koh, K.; Liu, G. J.; Willson, C. G. *J. Am. Chem. Soc.* **2006**, *128*, 15921–15927.
(60) Cameron, N. S.; Corbierre, M. K.; Eisenberg, A. *Can. J. Chem.* **1999**, *77*, 1311–1326.
(61) Bang, J.; Jain, S. M.; Li, Z. B.; Lodge, T. P.; Pedersen, J. S.; Kesselman, E.; Talmon, Y. *Macromolecules* **2006**, *39*, 1199–1208.
(62) Shen, H. W.; Eisenberg, A. *J. Phys. Chem. B* **1999**, *103*, 9473–9487.
(63) Nagarajan, R.; Ganesh, K. *J. Chem. Phys.* **1989**, *90*, 5843–5856.
(64) Zhulina, E. B.; Adam, M.; LaRue, I.; Sheiko, S. S.; Rubinstein, M. *Macromolecules* **2005**, *38*, 5330–5351.
(65) Underhill, R. S.; Ding, J. F.; Birss, V. I.; Liu, G. J. *Macromolecules* **1997**, *30*, 8298–8303.
(66) Brandrup, J.; Immergut, E. H. *Polymer Handbook*, 3rd ed.; John Wiley & Sons: New York, 1989; pp VII 3−47.
(67) Jain, S.; Bates, F. S. *Macromolecules* **2004**, *37*, 1511–1523.
(68) Forster, S.; Zisenis, M.; Wenz, E.; Antonietti, M. *J. Chem. Phys.* **1996**, *104*, 9956–9970.
(69) Battaglia, G.; Ryan, A. J. *J. Am. Chem. Soc.* **2005**, *127*, 8757–8764.
(70) Liu, F. T.; Eisenberg, A. *J. Am. Chem. Soc.* **2003**, *125*, 15059–15064.
(71) Luo, L. B.; Eisenberg, A. *Angew. Chem., Int. Ed.* **2002**, *41*, 1001+.
(72) Luo, L. B.; Eisenberg, A. *Langmuir* **2001**, *17*, 6804–6811.
(73) Stoenescu, R.; Meier, W. *Chem. Commun.* **2002**, 3016–3017.
(74) Magonov, S. N.; Elings, V.; Whangbo, M. H. *Surf. Sci.* **1997**, *375*, L385–L391.
(75) Wang, J.; Horton, J. H.; Liu, G. J.; Lee, S. Y.; Shea, K. J. *Polymer* **2007**, *48*, 4123–4129.
(76) Hu, J. W. N. G.; Liu, G. J. *Macromolecules* **2008**, in press.
(77) van Krevelen, D. W. *Properties of Polymers—Their Correlation with Chemical Structure; Their Numerical Estimation and Prediction from Additive Group Contributions*, 3rd ed.; Elsevier Science: Amsterdam, 1997.

MA801882R